A Broadband Achromatic Dielectric Planar Metalens in Mid-IR Range

Ye YUAN, Zilong YAN, Peifeng ZHANG, Zhu CHANG, Fengjiang PENG, Ruotong CHEN, Zhenyuan YANG, Shizheng CHEN, Qing ZHAO, and Xiaoping HUANG[*]

School of Resources and Environment, University of Electronic Science and Technology of China, Chengdu 610054, China

[*]Corresponding author: Xiaoping HUANG   E-mail: xphuang@uestc.edu.cn

Abstract: Metalens are planar lenses composed of the subwavelength arrays, which have unconventional and versatile functionalities to manipulate the light fields compared with the traditional lens. It is noted that the most metalens are designed in a monochromatic mode in the visible or mid-infrared range (mid-IR), however, the broadband range is needed in many practical applications, such as spectroscopy, sensing, and imaging. Here, we design and demonstrate a broadband achromatic dielectric metalens in the mid-IR range of 4 μm − 5 μm for near diffraction-limited (1.0λ) focusing. The broadband achromatic propagation and focusing of the metalens are designed and simulated by constructing and optimizing the phase profile. The Pancharatnam-Berry (P-B) phases of all the elements contribute to the main phase increment of the whole phase profile of the metalens. The additional phase is constructed and optimized by using the random search algorithm to obtain the optimized size of all the elements. The focusing efficiency of the achromatic metalens is also optimized and averaged as the result of phase optimization within a wide band for the building elements, while it is lowered comparing with the regular metalens without broadband achromatic designing. Using this combined designing approach, various flat achromatic devices with the broadband metalens can find a new way for full-color detection and imaging.

Keywords: Broadbands; achromatic; metalens; mid-IR

1. Introduction

The mid-infrared range (mid-IR) band of electromagnetic radiation is a particularly useful part of the spectrum [1–4]. It could enable a wide variety of applications, including thermal imaging, free-space communication, military navigation, and biomedical sensing [5–10]. However, the conventional optical components for the infrared band with the thick curved-glass lenses are hard to make, and the devices in this band are highly specialized and expensive. The metalens with planar metasurfaces provide a new perspective on flexibly shaping the light field by manipulating its phase and amplitude as well as polarization at will via a compact and easy-of-nanofabrication system [11–18]. At present, most of these metlenses are designed based on Pancharatnam-Berry (P-B) geometrical phases to adjust the phase profile and focus light beam at the particular wavelength

especially in the visible range. Besides that, there are some proposed metalenses with multispectral, dual-functional, and off-axis focusing that still exhibit large chromatic aberration, which is mainly resulted from the resonant phase dispersion of the building blocks and the intrinsic dispersion in the used materials [19–22]. Such chromatic aberration significantly degrades the performance of full-color optical applications, such as in communication, detection, navigation, and imaging. So, researchers use the structural dimensions for wavelengths selection [23–25] or add some phase compensation structures to achieve amplification or attenuation for some wavelengths, respectively [26–29]. In recent years, broadband achromatic metalenses have been intensively studied due to their great practical applications in industry products [30–32]. Up to now, there are about two categories of approaches to realize achromatic metalenses. One approach that is capable of eliminating the chromatic aberration at several discrete wavelengths of 1 300 nm, 1 550 nm, and 1 800 nm [19], is based on the low-loss dielectric resonators to introduce a dense spectrum of optical modes to enable dispersive phase compensation. The other approach to accomplish a broadband achromatic is to employ the integrated-resonant unit element in metasurfaces with smooth and linear phase dispersion combining with the geometric phase [26]. In addition, there is another approach to accomplish a high-efficiency broadband achromatic metalens for the near-IR biological imaging window [33]. The demonstrated metalens is composed of titanium dioxide nanopillars with record-high aspect ratios featuring pillar heights of 1.5 μm, which exhibits dramatically increased group delay range and broadband achromatism from 650 nm to 1 000 nm. In general, the phase profile of the wavefront determines the optical propagation in space. Therefore, to suppress the chromatic effect in a broad continuous bandwidth, the phase profile of the metalens should be designed strategically [33–35].

In this work, we propose a broadband achromatic planar metalens in the mid-IR range with a hybrid designing principle, which combines the P-B geometrical phases and additional phase. Herein, the P-B geometrical phases from all the elements rotation angle variation contribute to the main phase increment of the whole phase profile of the metalens. The additional phase is constructed and optimized by varing the length of all the elements. Through the combined designing method, a broadband achromatic dielectric metalens in the mid-infrared range of $4\,\mu m - 5\,\mu m$ for near diffraction-limited (1.0λ) focusing is designed and demonstrated. Here, the integrated resonant elements in the metalens represent the discrete P-B phase and linear phase response by simultaneously tailoring the orientation and the length of the dielectric rectangular resonant elements. Based on the waveguide theory, the effective medium theory, and generalized Snell's law, the propagation and focusing characteristics of the proposed planar metalens are simulated and calculated, which present the good achromatic performance in the mid-IR range of $4\,\mu m - 5\,\mu m$. The proposed devices are easily fabricated and significant for detecting techniques and biomedical applications in the mid-IR range.

2. Design, results, and discussion

Usually, IR materials such as Si or CaF_2 possess a merit of low absorption loss in the designed frequency [36]. To obtain the higher transmission efficiency at the mid-IR range, the all-dielectric resonant metalens of Si brick arrays on the CaF_2 substrate is used for our design. The optical transmission performance of the designed metalens is investigated and optimized in detail. The finite difference time-domain (FDTD) method is used to model the metalens and investigate its transmitting properties. The schematic diagram of the element structure is shown in Fig. 1(a), where a Si brick with the length l, the width w, and the height h is attached on the CaF_2 substrate. Here, the thickness of the

layer of the CaF$_2$ substrate is set as $0.5\,\mu m$. The width of the Si brick is fixed at $400\,nm$, and the length varies at the range of $600\,nm - 2\,000\,nm$. Here, for reducing calculation, we optimize the size of the nanobricks based on the effective medium theory while keeping the width of the Si brick is not changed. The height of the Si brick is $2\,500\,nm$, which is tall enough to cover 2π phase in the mid-infrared range [36]. Totally, the designed metalens is composed of a square lattice of Si brick arrays with a lattice constant of $2\,\mu m$. The boundary conditions in *x*, *y*, and *z* directions are set to the perfect match layer (PML), wherein the mesh size is set equally as $120\,nm$. The permittivities of Si and CaF$_2$ are taken from experimental results [37, 38]. The anisotropic feature of the Si brick is used to tailor the phase response to the incident circularly polarized light. Here, θ is the orientation angle between the long axis of the silica bar and the *x*-axis.
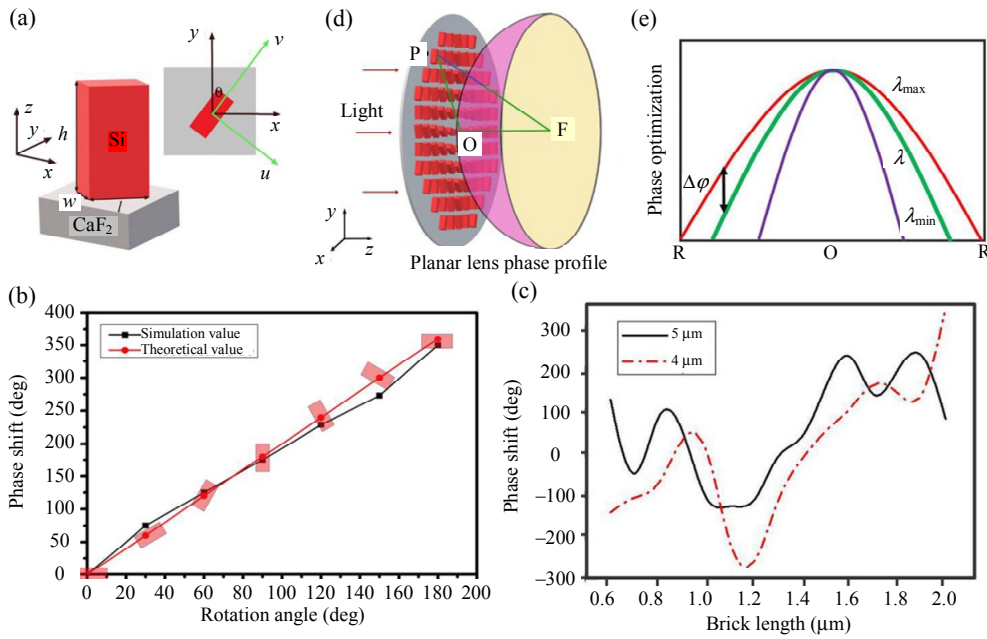

Fig. 1 Schematic diagram and phase tuning by the Si brick arrayed planar metalens: (a) a silicon brick on the CaF$_2$ substrate, $w = 400\,nm$, $h = 2\,500\,nm$, and *l* varies at the range of $600\,nm - 2\,000\,nm$ (the inset shows the brick orientation), (b) theoretical and simulation results of the phase response of the brick with different spatial orientations, (c) simulation results of the phase response of the nano-bricks with different lengths at the wavelengths of $4\,mm$ and $5\,mm$, (d) phase profile of the metalens composed of a square lattice of the Si brick arrays with a lattice constant of $s = 2\,\mu m$, and (e) phase distribution of different wavelengths at the same focus on lenses planes.

At first, the tailoring effect of a single Si brick on the phase and amplitude of the incident light with the circular polarization is studied. The two directions of the independent coordinate axes of the metalens structural unit are *u* and *v*, and the angle between the coordinate axis *u* and the *x*-axis of the reference coordinate system is θ. In the case of the circularly polarized light incidence, the electromagnetic fields after interaction with the metalens are expressed as [39]

$$\begin{bmatrix} E_{ox} \\ E_{oy} \end{bmatrix} = \frac{1}{2\sqrt{2}} \left\{ (t_u + t_v) \begin{bmatrix} 1 \\ j\sigma \end{bmatrix} + (t_u - t_v) e^{2j\sigma\theta} \begin{bmatrix} 1 \\ -j\sigma \end{bmatrix} \right\}$$

(1)

where $\pm\sigma$ represent the right-handed circular polarization and left-handed circular polarization. The transmittance coefficients of the electromagnetic waves in the two directions of *u* and *v* are t_u and t_v, respectively. It is easy to see that the scattered electromagnetic wave contains an origin polarized component and a component opposite to

the original polarization which carries $2\sigma\theta$ additional geometric phase. Importantly, this additional geometric phase is a key factor to realize the controllable wavefront reconstruction by the metalens. So, for $\sigma = 1$, when one rotates the Si nano-brick with discrete angles, it will bring the 2θ phase addition to the scattered field. In our design, a hybrid phase modulating method is used to construct the whole phase for the dielectric metalens. As shown in Fig. 1(b), a supercell with the seven Si bricks array covers 2π phase variation when the nano-brick presents a continuous rotation angle of $\pi/6$. The P-B geometrical phases of all the bricks contribute to the main phase increment of the whole phase profile of the metalens. In Fig. 1(c), the 2π phase response at the wavelengths of 4 mm and 5 mm versus the length of nano-bricks shows the dispersion values of the length of the nano-brick, where the brick sizes are $w = 400\,\text{nm}$, $h = 2\,500\,\text{nm}$, and l varies in the range of $600\,\text{nm} - 2\,000\,\text{nm}$.

Based on the phase constructing principle, the key process for achieving light focus by the planar metalens is to construct the desired phase plane. The distribution of phase increment at different positions for circular polarized incidences on the metalens is as following [40]:

$$\varphi(x_i, y_i) = \frac{2\pi}{\lambda_c}\left(f - \sqrt{x_i^2 + y_i^2 + f^2}\right) + 2n\pi \quad (2)$$

where λ_c is the central light wavelength, f is the focal length, n is an integer, and (x_i, y_i) represents the position on the plane of the lens. The design of a broadband achromatic metalens is to determine the phase profile required for the sub-diffraction focusing for different wavelengths. So, it is necessary to construct the phase profile as shown in Fig. 1(d) for different wavelengths. Accordingly, the phase profile for a broadband metalens at the arbitrary wavelength of $\lambda \in \{\lambda_{\min}, \lambda_{\max}\}$ should be designed to a parabolic profile, as shown in Fig. 1(e). Generally, in the case of the working wavelength range of $\lambda \in \{\lambda_{\min}, \lambda_{\max}\}$ and $\lambda_{\max}$ being the

boundaries of the interested wavelength, the phase in (2) can be rewritten as

$$\varphi_\lambda(x_i, y_i, \lambda) = \varphi_{\lambda\max}(x_i, y_i, \lambda_{\lambda\max}) + \Delta\varphi_{\lambda\max}(x_i, y_i, \lambda).$$
$$(3)$$

In the above formula, the first term on the right side of the equation is a fixed value as the reference wavelength and focal length are determined, which can be achieved by the P-B phase of the bricks in the metalens. The second is a wavelength-related term, which is determined by optimizing the size of the bricks based on the effective medium theory. Through the above phase construction processes, the final optimized metalens structures with a total phase corrections can be summed by the phase difference between the ideal phase and the real phase at each point (x_i, y_i), which is represented as

$$\Delta\varphi_{\text{total}} = \sum \Delta\varphi(\lambda) =$$
$$\sum_i \sum_n \varphi_I(x_i, y_i, \lambda_n) - \varphi_R(x_i, y_i, \lambda_n) \quad (4)$$

where the subscript i indicates a position (x_i, y_i) along the radius of the metalens, and λ_n is the wavelength range from $4\,\mu\text{m}$ to $5\,\mu\text{m}$. To obtain the optimal phase structure of the broadband achromatic metalens, the minimum value of the total phase corrections and the corresponding phase at each point need to be calculated. Because of the large data scale during the calculation, the random search algorithm with a strong searching ability is adopted in our simulation to analyze the x-axis phase response of the metalens with the designed focal length of $100\,\mu\text{m}$ and the diameter of $100\,\mu\text{m}$. In Fig. 2(a), the phase profiles at the positive x-axis side for several typical wavelengths are calculated through (2). In order to allow the metalens to work in a broadband frequency, the linear phase increases caused by optimizing the length of each brick to support the additional phase for the whole metalens. So, by using the hybrid phase modulating tactics for the metalens, the local response caused by changing the size of the brick and the non-local response caused by changing the position of the bricks

determines its transmission properties finally. The optimized phase profile at two represented wavelengths and the reference wavelength of 5 μm are shown in Figs. 2(b) – 2(d). Because the phase profile is optimized based on the reference wavelength of 5 μm, the phase difference between the ideal phase and the real phase at 5 μm is minimal. Compared to the ideal phase profile, the real optimized phase profiles are more meticulous, which can be fit to focus the light at a much broader band. Thus, the size and orientation for each Si brick along the radial direction are determined according to the phase requirement at each coordinate *r*. To

compensate the broadband dispersion, the minimum total phase corrections of (4) should be satisfied for each Si brick with the desired phase. In detail, the minimum phase should be obtained by calculating the phases for the bricks' length changes from 0.6 μm to 2 μm with an increment of 300 nm, where the wavelength increment is 0.2 μm. Then, the bricks' size at each coordinate *r* with the required phases can be determined. In general, the maximum conversion efficiency can be reached at a resonant wavelength. So, in a broadband range, the whole conversion efficiency of the metalens could be averaged and lowered.
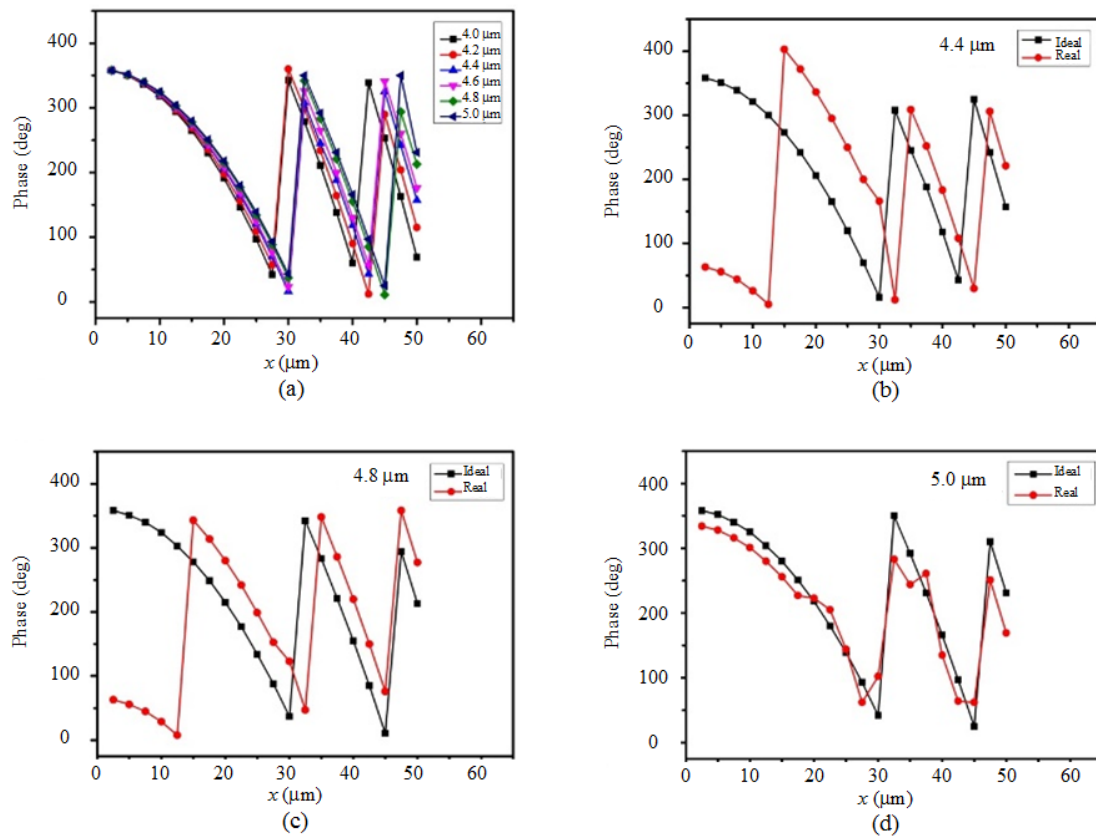

Fig. 2 Phase optimization: (a) theoretical ideal phase profile for some represented wavelengths at the positive *x*-axis of the lenses plane, and (b)–(d) ideal phase and real optimized phase at two represented wavelengths and the reference wavelength of 5 μm.

Now that the whole phase profile and dispersion are established, the nanostructures designing should be considered to simultaneously satisfy the required phase and group delay dispersion at each coordinate *r* in the metalens for all incidences. To compare, the regular metalens composed of Si bricks with the

same size is first constructed in Fig. 3(a). Then, the achromatic metalens with the desired phase profile is constructed by using an FDTD script method. To arrange the Si bricks on the CaF_2 substrate, the size and orientation for each Si brick at a certain coordinate *r* are based on the calculation results. By

changing the length of the bricks with the fixed width of 400 nm and the thickness of 2 500 nm, the optimized metalens with the desired phase profile is constructed. As shown in Fig. 3(b), the elements are arranged into a circular shape with a fixed radius, which is corresponded to the circle radius of the projection of the phase profile to the substrate. After the arrangement circle by circle, the whole metalens is constructed finally with a diameter of 100 μm on the CaF$_2$ substrate. In Fig. 3(c), the enlarged image shows the clear arrangements of the elements. Each element supports a particular light scattering and controls the phase of the scattered light field by its orientation and geometrical shape.
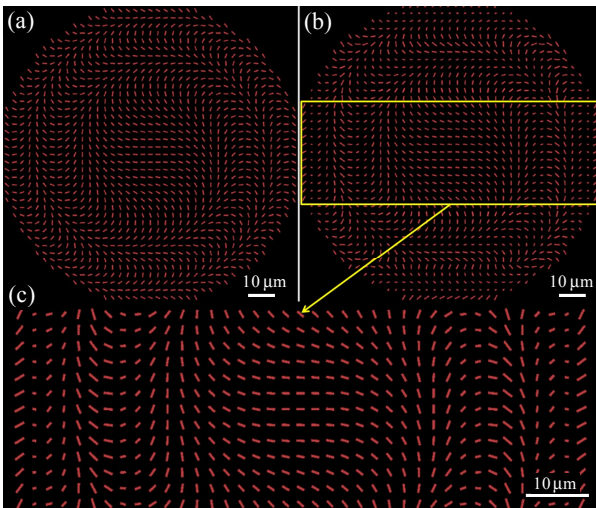

Fig. 3 Schematic diagram of the metalens with the Si bricks: (a) regular metalens composed of the Si bricks with the same size of w = 400 nm, l = 1 600 nm, and h = 2 500 nm, (b) achromatic metalens with the Si bricks arranged with the desired phase profile, where the width is 400 nm and the thickness is 2 500 nm, and the length varies at the range of 600 nm – 2 000 nm, and (c) enlarged area notifies the clear arrangements of the elements in (b).

For the practical applications of focusing devices with the broadband achromatic property, the operational bandwidth should be investigated and analyzed. To investigate the broadband characteristics of our metalens, the performance of achromatic focusing is simulated for the design at the incident wavelength range of 4 μm – 5 μm. Together, the broadband focusing performance of the regular metalens is chosen to compare. The numerical aperture (NA) variation of two kinds of

designed metalens with a diameter of 100 μm for different wavelengths is illustrated in Fig. 4(a). In addition, we have also simulated a metalens with a diameter of 80 μm and a focal length of 20 μm, where the full-width at half-maximum (FWHM) value is 4.5 μm. So, the NA value of the metalens is about 0.89. Then, we get the theoretical resolution limit of 2.74 μm for the lens, which is about 1.6 times of the diffraction limit. Therefore, it is difficult to increase the NA value as the diameter increases, while the focal length and phase profile of the metalens are fixed. The focal length for normal incidences at the wavelength range of 4 μm – 5 μm for the regular metalens and achromatic metalens is depicted in Fig. 4(b). The simulated intensity distributions in the linear scale of the focal profile at different wavelengths in the case without and with the phase optimization are shown in Figs. 4(c) and 4(d), respectively. It is observed that the focal planes of the achromatic metalens with the phase optimization are almost located at a small range of 105 μm to 116 μm, which is very near to the designed focal length of 100 μm. Together, the intensity distribution of the focal profile varies little. In contrast, for the regular metalens without the phase optimization, the focal planes shift dramatically from 100 μm to 125 μm and the intensity distribution of the focal profile varies clearly. We ascribe this focusing performance difference to the hybrid phase modulating for the metalens. At the same time, the resonant dispersion between nanoblocks with different sizes also plays a role in achieving a broadband achromatic metalens [41, 42]. Figure 4(e) shows the simulated intensity profiles along the white dashed lines in Figs. 4(c) and 4(d) at different wavelengths, which is also demonstrated to visualize the effect of chromatic aberration of the two kinds of metalens. Through the calculation, it can be found that the FWHM of the focus spot reaches the smallest value of 1.0λ. Here, since the benchmark phase profile and dispersion

optimization are chosen at the wavelength of 5 μm, the focusing efficiency at 5 μm is the highest, and it slightly decreases from 5 μm to 4 μm. We attribute the superior broadband characteristics of our

metalens in the range of 4 μm – 5 μm to the fact that the phase control relies on not only the orientations of the bricks but also the elements length tuning at different incident wavelengths.
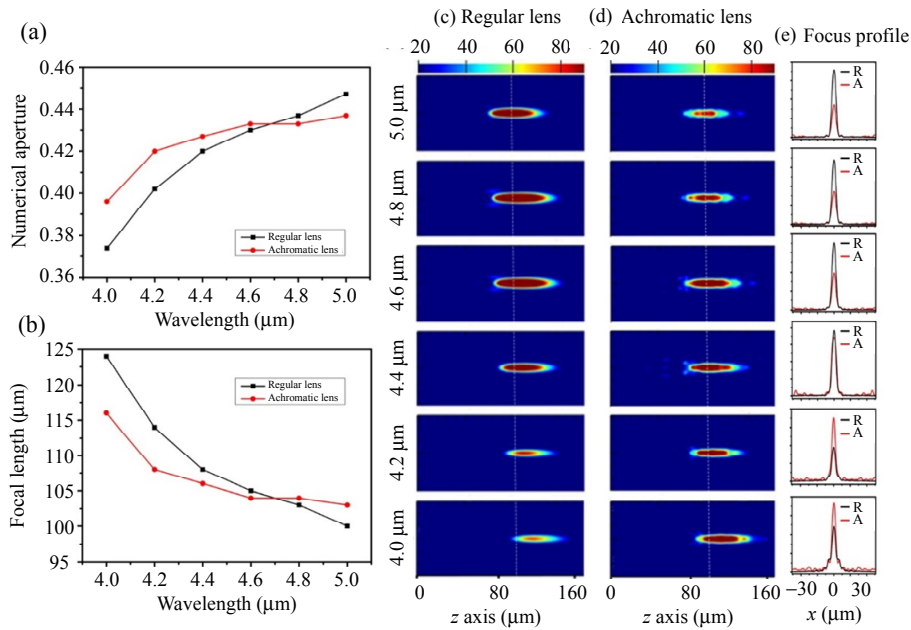

Fig. 4 Focusing performance of the regular metalens and the achromatic metalens: (a) numerical aperture variation of the designed metalens for different wavelengths, (b) focal length for normal incidences at the wavelength range of 4 μm – 5 μm; simulated results of the intensity distribution in the linear scale of the focal profile at different wavelengths in the case of without (c) and with the phase optimization (d); (e) simulated intensity profiles along the white dashed lines in Figs. 4(c) and 4(d) at different wavelengths to visualize the effect of chromatic aberration of the regular metalens and achromatic metalens.

To compare the focusing performance of the metalens, the focusing efficiencies of the regular metalens and achromatic metalens are calculated at different wavelengths in the mid-infrared range. The focusing efficiency is calculated with the ratio of the intensity integral of the FWHM and the whole intensity profile at the focal plane as shown in the inset of Fig. 5. As shown in Fig. 5, the focusing efficiency of the regular metalens reaches a highest value of 72% at 5 μm. However, the focusing efficiency drops gradually when the wavelength varies from 5 μm to 4 μm. For the achromatic metalens, the highest efficiency is up to 62%, while the average efficiency is about 51.6% over the whole working bandwidth. Mostly, this focusing efficiency average process of the achromatic metalens is the result of the phase optimization of the building elements. The phase optimization in a

broad band range from 4 μm to 5 μm causes more energy to be reflected and absorbed, so the overall focusing efficiency of metalens is averaged and lower than that of the regular metalens at some particular wavelengths.
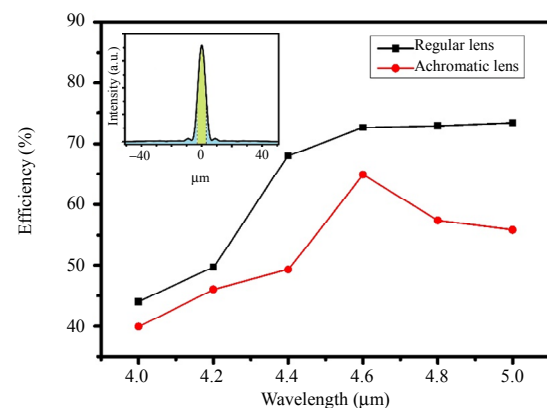

Fig. 5 Focusing efficiency of the regular metalens and achromatic metalens under different wavelengths in the mid-infrared range. The inset is the focusing efficiency schematic diagram.

3. Conclusions

In conclusion, we have proposed and demonstrated a novel metalens that are capable of a broadband chromatic focusing in the mid-IR range. These metalenses utilize the arrangement orientation and length variation of the bricks to form an accurate phase profile for correcting chromatic aberration. The demonstrated results show that these metalenses render a good achromatic performance in the mid-IR range of $4\,\mu m - 5\,\mu m$. Our presented metalens that can be used for broadband achromatic focusing in the mid-IR band, which has high potential applications of ultra-compact imaging, spectroscopy, and detection in the infrared range. Moreover, our design scheme is an effective and robust way for the phase encoding and wavefront modulating in the metalens design and fabrication.

Acknowledgment

References

[1] L. Zhang, J. Ding, H. Y. Zheng, S. S. An, H. T. Lin, B. W. Zheng, *et al.*, "Ultra-thin high-efficiency mid-infrared transmissive Huygens meta-optics," *Nature Communications*, 2018, 9(1): 1–9.
[2] Y. Yang, Q. Zhao, L. Liu, Y. Liu, C. Rosales-Guzmán, and C. W. Qiu, "Manipulation of orbital-angular-momentum spectrum using pinhole plates," *Physical Review Applied*, 2019, 12(6): 064007.
[3] P. Sun, M. Zhang, F. Dong, L. Feng, and W. Chu, "Broadband achromatic polarization insensitive metalens over 950 nm bandwidth in the visible and near-infrared," *Chinese Optics Letters*, 2022, 20(1): 013601.
[4] Y. Cui, G. Zheng, M. Chen, Y. Zhang, Y. Yang, J. Tao, *et al.*, "Reconfigurable continuous-zoom metalens in visible band," *Chinese Optics Letters*, 2019, 17(11): 111603.
[5] F. F. Li, H. J. Liu, N. Huang, and Z. L. Wang, "Near infrared step-zoom doublet lens based on dielectric metasurfaces," *Journal of Optics*, 2018, 20(7): 075105.
[6] M. Khorasaninejad and F. Capasso, "Metalens: versatile multifunctional photonic components," *Science*, 2017, 358: 1146.
[7] S. Y. Zhang, M. H. Kim, F. Aieta, A. She, T. Mansuripur, I. Gabay, *et al.*, "High efficiency near diffraction-limited mid-infrared flat lenses based on metasurface reflectarrays," *Optics Express*, 2016, 24(16): 18024–18034.
[8] A. Wang, Z. M. Chen, and Y. P. Dan, "Planar metalens in the mid-infrared," *AIP Advances*, 2019, 9(8): 085327.
[9] T. Liu, J. Hu, L. Zhu, R. Zhou, C. Zhang, C. Wang, *et al.*, "Large effective aperture metalens based on optical sparse aperture system," *Chinese Optics Letters*, 2020, 18(10): 100001.
[10] Y. Zhao, Y. Su, X. Hou, and M. Hong, "Directional sliding of water: biomimetic snake scale surfaces," *Opto-Electronic Advances*, 2021, 4(4): 04210008.
[11] M. Khorasaninejad, W. T. Chen, R. C. Devlin, J. Oh, A. Y. Zhu, and F. Capasso, "Metalens at visible wavelengths: diffraction-limited focusing and subwavelength resolution imaging," *Science*, 2016, 352: 1190–1194.
[12] C. Saeidia and D. V. D. Weide, "Wideband plasmonic focusing metasurfaces," *Applied Physics Letters*, 2014, 105(5): 053107.
[13] H. S. Ee and H. G. Park, "Design of tunable silicon metasurfaces with cross-polarization transmittance over 80%," *Physica Scripta*, 2018, 93(8): 085501.
[14] R. Z. Li, F. Shen, Y. X. Sun, W. Wang, L. Zhu, and Z. Y. Guo, "Broadband, high-efficiency, arbitrary focusing lens by a holographic dielectric meta-reflectarray," *Journal of Physics D: Applied Physics*, 2016, 49(14): 145101.
[15] F. Zhang, H. L. Yu, J. W. Fang, M. Zhang, S. C Chen, J. Wang, *et al.*, "Efficient generation and tight focusing of radially polarized beam from linearly polarized beam with all-dielectric metasurface," *Optics Express*, 2016, 24(6): 6656–6664.
[16] M. K. Chen, Y. F. Wu, L. Feng, Q. B. Fan, M. H. Lu, T. Xu, *et al.*, "Principles, functions, and applications of optical meta-lens," *Advanced Optical Materials*, 2021, 9(4): 2001414.
[17] L. Li, Z. X. Liu, X. F. Ren, S. M. Wang, V. Su,

M. K. Chen, *et al.*, "Metalens-array-based high-dimensional and multiphoton quantum source," *Science*, 2020, 368(6498): 1487–1490.

[18] M. X. Zhao, M. K. Chen, Z. P. Zhuang, Y. W. Zhang, A. Chen, Q. M. Chen, *et al.*, "Phase characterization of metalens," *Light: Science & Applications*, 2021, 10(4): 551–561.

[19] F. Aieta, M. A. Kats, P. Genevet, and F. Capasso, "Multiwavelength achromatic metasurfaces by dispersive phase compensation," *Science*, 2015, 347(6228): 1342–1345.

[20] Q. Wang, X. Q. Zhang, Y. H. Xu, Z. Tian, J. Q. Gu, W. S. Yue, *et al.*, "A broadband metasurface-based terahertz flat-lens array," *Advanced Optical Materials*, 2015, 3(6): 779–785.

[21] H. W. Liang, Q. L. Lin, X. S. Xie, Q. Sun, Y. Wang, L. D. Zhou, *et al.*, "Ultrahigh numerical aperture metalens at visible wavelengths," *Nano Letters*, 2018, 18(7): 4460–4466.

[22] A. Arbabi, Y. Horie, M. Bagheri, and A. Faraon, "Dielectric metasurfaces for complete control of phase and polarization with subwavelength spatial resolution and high transmission," *Nature Nanotechnology*, 2015, 10(11): 937–943.

[23] K. Li, Y. I. Guo, M. B. Pu, X. Li, X. L. Ma, Z. Y. Zhao, *et al.*, "Dispersion controlling meta-lens at visible frequency," *Optics Express*, 2017, 25(18): 21419–21427.

[24] N. F. Yu and F. Capasso, "Flat optics with designer metasurfaces," *Nature Materials*, 2014, 13: 139–140.

[25] Z. Li, E. Palacio, S. Butun, and K. Aydin, "Visible-frequency metasurfaces for broadband anomalous reflection and high-efficiency spectrum splitting," *Nano Letters*, 2015, 15(3): 1615–1621.

[26] S. M. Wang, P. C. Wu, S. Vin-Cent, L. Yi-Chieh, C. H. Chu, C. Jia-Wern, *et al.*, "Broadband achromatic optical metasurface devices," *Nature Communications*, 2017, 8(1): 1–9.

[27] M. Khorasaninejad, F. Aieta, P. Kanhaiya, M. A. Kats, P. Genevet, D. Rousso, *et al.*, "Achromatic metasurface lens at telecommunication wavelengths," *Nano Letters*, 2015, 15(8): 5358–5363.

[28] D. Lin, P. Y. Fan, E. Hasman, and M. L. Brongersma, "Dielectric gradient metasurface optical elements," *Science*, 2014, 345(6194): 298–302.

[29] H. H. Hsiao, Y. H. Chen, R. J. Lin, P. C. Wu, S. M. Wang, B. H. Chen, *et al.*, "Integrated resonant unit of metasurfaces for broadband efficiency and phase manipulation," *Advanced Optical Materials*, 2018, 6(12): 1800021.

[30] K. Ou, F. L. Yu, G. H. Li, W. J. Wang, A. E. Miroshnichenko, L. J. Huang, *et al.*, "Mid-infrared polarization-controlled broadband achromatic metadevice," *Science Advances*, 2020, 6(37): eabc0711.

[31] S. Shrestha, A. C. Overvig, M. Lu, A. Stein, and N. F. Yu, "Broadband achromatic dielectric metalens," *Light: Science & Applications*, 2018, 7(1): 1–11.

[32] Z. J. Zhang, Z. C. Cui, Y. Liu, S. C. Wang, I. Staude, Z. Y. Yang, *et al.*, "Design of a broadband achromatic dielectric metalens for linear polarization in the near-infrared spectrum," *OSA Continum*, 2018, 1(3): 882–890.

[33] Y. J. Wang, Q. M. Chen, W. H. Yang, Z. H. Ji, L. M. Jin, X. Ma, *et al.*, "High-efficiency broadband achromatic metalens for near-IR biological imaging window," *Nature Communications*, 2021, 12(1): 1–7.

[34] S. Wang, P. C. Wu, V. C. Su, Y. C. Lai, M. K. Chen, H. Kuo, *et al.*, "A broadband achromatic metalens in the visible," *Nature Nanotechnology*, 2018, 13(3): 227–232.

[35] W. Chen, A. Y. Zhu, V. Sanjeev, M. Khorasaninejad, Z. Shi, E. Lee, *et al.*, "A broadband achromatic metalens for focusing and imaging in the visible," *Nature Nanotechnology*, 2018, 13(3): 220–226.

[36] Z. L. Guo, L. H. Tian, F. Shen, H. P. Zhou, and K. Guo, "Mid-infrared polarization devices based on the double-phase modulating dielectric metasurface," *Journal of Physics D: Applied Physics*, 2017, 50(25): 254001.

[37] D. Chandler-Horowitz and P. M. Amirtharaj, "High-accuracy, midinfrared ($450 \text{ cm}^{-1} \leq \omega \leq 4\,000 \text{ cm}^{-1}$) refractive index values of silicon," *Journal of Applied Physics*, 2005, 97(12): 123526.

[38] M. Herzberge and C. D. Salzber, "Refractive indices of infrared optical materials and color correction of infrared lenses," *Journal of the Optical Society of America*, 1962, 52(4): 420–427.

[39] W. T. Chen, A. Y. Zhu, J. Sisler, Y. W. Huang, K. M. A. Yousef, E. Lee, *et al.*, "Broadband achromatic metasurface-refractive optics," *Nano Letters*, 2018, 18(12): 7801–7808.

[40] F. Aieta, P. Genevet, M. A. Kats, N. F. Yu, R. Blanchard, Z. Gaburro, *et al.*, "Aberration-free ultrathin flat lenses and axicons at telecom wavelengths based on plasmonic metasurfaces," *Nano Letters*, 2012, 12(9): 4932–4936.

[41] W. H. Ni, X. H. Kou, Z. Yang, and J. F. Wang, "Tailoring longitudinal surface plasmon wavelengths, scattering and absorption cross sections of gold nanorods," *ACS Nano*, 2009, 2(4): 677–686.

[42] W. Su, X. Y. Li, J. Bornemann, and R. Gordon, "Theory of nanorod antenna resonances including end-reflection phase," *Physical Review B*, 2015, 91(16): 165401.